ADAPTIVE NUMERICAL-DISSIPATION/FILTER CONTROLS FOR HIGH ORDER NUMERICAL METHODS

H. C. YEE
NASA Ames Research Center, Moffett Field, CA 94035, USA

AND

B. SJÖGREEN
Department of Numerical Analysis and Computer Sciences, KTH, 100 44 Stockholm, Sweden

Abstract.[1] Proper control of the numerical-dissipation/filter to accurately resolve all relevant multiscales of complex flow problems while still maintaining nonlinear stability and efficiency for long-time numerical integrations poses a great challenge to the design of numerical methods. The required type and amount of numerical-dissipation/filter are not only physical problem dependent, but also vary from one flow region to another. An approach for the automatic detection of different flow features as distinct sensors to signal the appropriate type and amount of numerical-dissipation/filter for non-dissipative high order schemes is proposed. These scheme-independent sensors are capable of distinguishing shocks/shears, turbulent fluctuations and spurious high-frequency oscillations. In addition, these sensors are readily available as an improvement over existing grid adaptation indicators. The same shock/shear detector that is designed to switch on the shock/shear numerical dissipation can be used to switch off the entropy splitting form of the inviscid flux derivative [31] in the vicinity the discontinuous regions to further improve nonlinear stability and minimize the use of numerical dissipation. The rest of the sensors in conjunction with the local flow speed and Reynolds number can also be used to adaptively determine the appropriate entropy splitting parameter for each flow type/region. The goal of this paper is to further improve nonlinear stability, accuracy and efficiency of long-time numerical integration of complex shock/turbulence/acoustics interactions and numerical combustion. The minimization of employing very fine grids to overcome the production of spurious numerical solution and/or instability due to under-resolved grids is also sought [29, 6].

1. Motivation and Objective

When employing finite time steps and finite grid spacings in the long-time integration of multiscale complex nonlinear fluid flows, nonlinear instability commonly occurs and the use of a numerical-dissipation/filter is unavoidable. Aside from acting as a post-processor step, most filters serve as some form of numerical dissipation. Without loss of generality, "numerical-dissipation/filter" is, hereafter, referred to as "numerical dissipation" unless otherwise stated. The required type and amount of numerical dissipation can vary drastically from one flow region to another (within the same problem) and are highly problem dependent. This is particularly

[1]Proceedings of the Third AFOSR International Conference on DNS/LES, Arlington, Texas, August 4-9, 2001. Part of this work was carried out while the second author was a visiting scientist with RIACS, NASA Ames Research Center.

true for unsteady high-speed turbulence and/or combustion problems. For this type of problem, it is of paramount importance to have proper control on the type and amount of numerical dissipation in regions where it is needed but nowhere else. Inappropriate type and/or amount can be detrimental to the integrity of the computed solution, especially for problems with no known analytical solution and/or experimental data for comparison.

The linear and nonlinear numerical dissipation presently available is either built into the numerical scheme or added on to the existing scheme. The built-in numerical dissipation schemes are, e.g., upwind, flux corrected transport (FCT), total variation diminishing (TVD), essentially non-oscillatory (ENO), weighted ENO (WENO), and hybrid schemes (e.g., those that switch between spectral and high-order shock-capturing schemes). The built-in nonlinear numerical dissipation in TVD, ENO and WENO schemes was designed to capture accurately discontinuities and high gradient flows while hoping to maintain the order of accuracy of the scheme away from discontinuities.

There exist different specialized linear and nonlinear filters to post process the numerical solution after the completion of a full time step of the numerical integration. Since they are post processors, the physical viscosity, if it exists, is taken into consideration. The main design principle of linear filters is to improve nonlinear stability, under-resolved grids [6] and de-aliasing of smooth flows, while the design principle of nonlinear filters is to improve the nonlinear stability and accuracy near discontinuities as well. See, for example, the present proceedings and [9, 6, 7, 27] for forms of linear filters, and see [30, 31, 21] for forms of nonlinear filters. For direct numerical simulation (DNS) and large eddy simulation (LES), there are additional variants of the filter approach.

For the last decade, CPU intensive high order schemes with built-in nonlinear dissipation have been gaining in popularity in DNS and LES for long-time integration of shock-turbulence interactions. Unfortunately, these built-in dissipations cannot clearly distinguish shocks/shears, from turbulent fluctuations and/or spurious high-frequency oscillations. In [30, 31, 21], it was shown that these built-in numerical dissipation are more dissipative and less accurate than the nonlinear filter approach of [30, 31, 21] with a similar order of accuracy. It was also shown that these nonlinear filters can also suppress spurious high-frequency oscillations. However, a subsequent study of Sjögreen & Yee [23] showed that the high order linear filter can sustain longer time integration more accurately than the nonlinear filter for low speed smooth flows. In other words, for the numerical examples that were examined in [23], the high order linear filter can remove high-frequency oscillations producing nonlinear instability better than the second-order nonlinear filter. Higher than third-order nonlinear filters might be able to improve their performance or might outperform the high order linear filters at the expense of more CPU time and added complexity near the computational boundaries. These findings prompted the design of switching on and off or blending of different filters to obtain the optimal accuracy of high order spatial difference operator as proposed in Yee et al. and Sjögreen & Yee [31, 21]. The missing link of what was proposed in [31, 21] is an efficient, automated and reliable set of appropriate sensors that are capable of distinguishing shocks/shears, from turbulent fluctuations and/or spurious high-frequency oscillations for a full spectrum of flow speeds and Reynolds numbers.

The present paper is a sequel to [30, 31, 21]. The objective here is to propose an adaptive procedure employing appropriate sensors to switch on the desired numerical dissipation where needed and leave the rest of the region free of numerical dissipation contamination while at the same time improving nonlinear stability of the entire numerical process. In addition, the minimization of employing very fine grids to overcome the production of spurious numerical solutions and/or instability due to under-resolved grids is sought [6]. It was shown in [17, 8, 31, 21] that conditioning the governing equations via entropy splitting of the inviscid flux derivatives [31] can improve the over all stability of the numerical approach for smooth flows. Therefore, the same shock/shear detector that is designed to switch on the shock/shear numerical dissipation can be used to switch off the entropy splitting form of the inviscid flux derivative in the vicinity the

discontinuous regions to further improve nonlinear stability and minimize the use of numerical dissipation. The rest of the sensors, in conjunction with the local flow speed and Reynolds number, can also be used to adaptively determine the appropriate entropy splitting parameter for each flow type/region. These sensors are readily available as an improvement over existing grid adaptation indicators. If applied correctly, the proposed adaptive numerical dissipation control is scheme independent, and can be a stand alone option for many of the favorite schemes used in the literature. Although the proposed adaptive procedure is scheme independent, we prefer a complete treatment of the numerical approach in the following framework:

1. For stability considerations, condition the governing equations before the application of the appropriate numerical scheme.
2. For consistency, compatible schemes that posses stability properties similar to those of the discrete analogue of the continuum are preferred.
3. For the minimization of numerical dissipation contamination, efficient and adaptive numerical dissipation control to further improve nonlinear stability and accuracy should be used.
4. For practical considerations, the numerical approach should be efficient and applicable to general geometries. An efficient and reliable dynamic grid adaptation should be used if necessary. Note that the computation of the illustrative examples used such a numerical approach [30, 31, 28, 21, 8, 16].

A brief summary of (1)-(3) is discussed in the next three sections. Some representative examples to illustrate the performance of the approach are given in Section 5.

2. Conditioning of the Governing Equations

Traditionally, conditioning the governing partial differential equations (PDEs) usually referred to rewriting the governing equations in an equivalent set of PDEs in order to prove the stability and/or well-posedness of the PDEs. When numerical methods are used to solve PDEs that are nonlinear, it is well-known that different equivalent forms of the governing equations might exhibit different numerical stability, accuracy and/or spurious computed solutions, even for problems containing no shock/shear discontinuities. There are many conditioned forms of the governing equations proposed in the literature. Different conditioned forms of the convection fluxes and the viscous fluxes have been proposed for the incompressible and compressible Navier-Stokes equations. Here we mention a few which are precursors of the so called entropy splitting of the compressible Euler equations [31]. If a method-of-lines approach is used to discretize these equations, the entropy splitting reduces to the splitting of the convection flux derivatives.

The splitting of the convection terms (for both the compressible and incompressible Navier-Stokes equations) into a conservative part and a non-conservative part has been known for a long time. In the DNS, LES and atmospheric science simulation literature, it is referred to as the skew-symmetric form of the momentum equations [1, 14, 2, 35]. It consists of the mean average of the conservative and non-conservative (convective form [35]) part of the momentum equations. The spatial difference operator is then applied to the split form. From the numerical analysis standpoint, the Hirt and Zalesak's ZIP scheme [12, 34] is equivalent to applying central schemes to the non-conservative momentum equations (convective form of the momentum equations). MacCormack [15] proposed the use of the skew-symmetric form for problems other than DNS and LES. Harten [10] and Tadmor [26] discussed the symmetric form of the Euler equations and skew-adjoint form of hyperbolic conservation laws, respectively. Although the derivation in these works is different, the ultimate goal of using the split form is almost identical. This goal is to improve nonlinear stability, minimize spurious high-frequency oscillations and robustness of the numerical computations. See [33, 23] for a historical consolidation of these approaches. The canonical splitting used by Olsson & Oliger [17] is a mathematical tool to prove the existence of a generalized energy estimate for a symmetrizable system of conservation laws. For the ther-

mally perfect gas compressible Euler equations, the transformation consists of a convex entropy function that satisfies a mathematical entropy condition. The mathematical entropy function, in this case, can be a function of the physical entropy. Therefore, the resulting splitting was referred to as **entropy splitting** for ease of reference by Yee et al. [31]. The entropy splitting can be viewed as the more general form which provides L_2 stability proof of the nonlinear Euler equations with physical boundary conditions included.

Consider a general nonlinear system of conservation laws,

$$U_t + F(U)_x = 0, \quad a \le x \le b. \tag{2.1}$$

If the conservation law has an entropy function, it can be transformed into a symmetric conservation law in terms of a new variable W. The change of variables $\partial U/\partial W$ is symmetric and positive definite, and the new Jacobian $\partial F/\partial W$ is symmetric. If furthermore U and F are homogeneous in W of degree β, which is the case for the thermally perfect gas Euler equations for any $\beta \neq -1$, the formulas become simple. In that case we insert the change of variables into the conservation law, and define the split form of the flux derivative [17]

$$U_t + \frac{\beta}{1+\beta} F_x + \frac{1}{1+\beta} F_W W_x = 0, \tag{2.2}$$

with β a splitting parameter ($\beta = \infty$ recovers the original conservative form). Here $\beta \neq -1$ and, for a perfect gas, $\beta > 0$ or $\beta < \frac{\gamma}{1-\gamma}$. The theory only gives the range of β and does not give any guidelines on how to choose β for the particular flow. The vectors F_W and W can be cast as functions of the primitive variables and β. From the study of [31], β is highly problem dependent. Multiplying the above equation by W (where $(\mathbf{p}, \mathbf{q})$ denotes the scalar or inner product of the vectors $\mathbf{p}$ and $\mathbf{q}$), gives

$$-(1+\beta)(W, U_t) = \beta(W, F_x) + (W, F_W W_x) = \beta(W, F_x) + (F_W W, W_x). \tag{2.3}$$

Integration by parts in space gives

$$(1+\beta)(W, U_t) = -[W^T F_W W]_a^b \tag{2.4}$$

from which we obtain the estimate

$$\begin{aligned} \tfrac{d}{dt}(W, U_W W) = \; & (W_t, U_W W) + (W, (U_W W)_t) = (U_t, W) + \beta(W, U_t) = \\ & (1+\beta)(W, U_t) = -[W^T F_W W]_a^b. \end{aligned} \tag{2.5}$$

In order to have an energy estimate, the boundary term $[W^T F_W W]_a^b$ should be of the sign that makes the time derivative of the norm negative. For stability the entropy norm $(W, U_W W)$ should be bounded.

3. Discrete Analogue of the Continuum

For ease of reference, "scheme" or more precisely "interior scheme" here generally refers to spatial difference schemes for the interior grid points of the computational domain, whereas "boundary scheme" is the numerical boundary difference operators for grid points near the boundaries. However, without loss of generality, we also adopt the conventional terminology of denoting "scheme" interchangeably as either the "combined interior and boundary scheme" or just the "interior scheme" within the context of the discussion. Before 1994, rigorous stability estimates for accurate and appropriate boundary schemes associated with fourth-order or higher spatial interior schemes were the major stumbling block in the theoretical development of combined interior and boundary schemes for nonlinear systems of conservation laws. Olsson [18] proved

that an energy estimate can be established for second-order central schemes. To obtain a rigorous energy estimate for high order central schemes, one must apply the scheme to the split form of the inviscid governing equation. A discrete analogue of the continuum using a semi discrete approach can be written as

$$\frac{dU_j(t)}{dt} = -\frac{\beta}{1+\beta} DF(U_j) - \frac{1}{1+\beta} F_W(U_j) DW_j. \tag{3.1}$$

Here, D is a difference operator, having the summation by parts (SBP) property [18, 25]. The estimate

$$\frac{d}{dt}(W, U_W W)_h = -W_J^T F_W(W_J) W_J + W_1^T F_W(W_1) W_1 \tag{3.2}$$

in the discrete scalar product follows in the same way as for the PDE with indices 1 and J the end points of the computational domain, and h the grid spacing. Here the SBP satisfying difference operator, for example, consists of central difference interior operators of even order together with the corresponding numerical boundary operators that obey the discrete energy estimate. See Olsson and Strand for forms of the SBP boundary operators [18, 25].

For the full discretization of the problem, we should discretize in time in such a way that the discrete energy estimate also holds. The obvious solution would be to discretize in time in a skew symmetric way, in a manner similar to the spatial discretization, e.g.,

$$\frac{\beta}{1+\beta} D_t U_j^n + \frac{1}{1+\beta} U_W(W_j^n) D_t W_j = -\frac{\beta}{1+\beta} DF(U_j^n) - \frac{1}{1+\beta} F_W(W_j^n) DW_j^n. \tag{3.3}$$

However, it turns out that the SBP property of the time difference quotient leads to a problem which is coupled implicitly in the time direction. To solve it we have to solve a nonlinear system of equations for all time levels in the same system, leading to an impractically large computational effort. Furthermore, numerical experiments shown in Sjögreen & Yee [23] indicated that a bounded L^2 entropy norm $(W, U_W W)_h$ does not necessarily guarantee a well behaved numerical solution for long-time integrations. In other words, L^2 stability does not necessarily guarantee an accurate solution. In practical computations, the classical Runge-Kutta time discretizations using the method-of-lines approach (which we used for our numerical experiments) works well, but we have not been able to prove a time discrete entropy estimate for this method. In addition, numerical experiments shown in [23] indicate that the time discrete problem does not have a decreasing entropy norm for all values of β. Numerical experiments in Yee et al. [31, 19] also indicate the wide variations of the β value for a full spectrum of flow problems. For example, if a constant β is used for problems containing shock waves, a very large value of β is needed. Otherwise diverge solution or wrong shock location and/or shock strength are obtained. With these findings, employing a constant β (within the allowable range of β) throughout the entire computational domain is not advisable unless the flow problem is a simple smooth flow. Studies in [31, 21] indicate that the split form of the inviscid flux derivatives does help in minimizing the use of numerical dissipation. What is needed is adaptive control of the β parameter from one flow region to another as well as from one physical problem to another.

We would like to point out that for non-homogeneous physical boundary conditions, it is important to impose these boundary conditions to maintain the SBP property. For a nonlinear symmetrizable system of conservation laws that contain time-dependent physical boundary conditions, an extra complication arises, especially if a multistage Runge-Kutta method is used. See Johansson [13] for a discussion.

4. Adaptive Numerical Dissipation Control

For smooth flows, entropy splitting does significantly improve the stability of the computation, but does not completely remove all nonlinear instabilities, especially for long-time wave

propagations, computation of turbulent statistics, and spurious numerical solutions and spurious oscillations due to under-resolved grids [29, 6]. Furthermore, the entropy splitting was developed for smooth solutions. Additional difficulties from shock wave formation are the oscillatory behavior of the centered difference interior scheme, and the fact that the nonconservative terms might lead to inconsistent behavior at shocks/shears [31, 21, 23]. We propose to enhance the above conditioning of the equations with an advanced numerical dissipation model, which includes nonlinear sensors to detect shocks/shears and other small scale features, and spurious oscillation instability due to under-resolved grids. Furthermore, we will use the detector to switch off the entropy splitting at shocks/shears and adjust the entropy splitting parameter with the aid of local Mach number and Reynolds number in smooth region as discussed earlier. The advanced numerical dissipation model can be used: (Option I) as part of the scheme, (Option II) as an adaptive filter control after the completion of a full time step of the numerical integration or (Option III) as a combination of Options I and II (e.g., high order nonlinear dissipation (with sensor control) using Option I and nonlinear filter (with a different sensor control) using Option II).

Due to space constraints, we concentrate here on an adaptive procedure that can distinguish three major computed flow features to signal the correct type and amount of numerical dissipation needed in addition to controlling the entropy splitting parameter. The major flow features and numerical instability are (a) shocks/shears , (b) turbulent fluctuations , and (c) spurious high-frequency oscillations. The procedure can be extended if additional refinement or classification of flow types and the required type of numerical dissipation is needed. There exist different detection mechanisms in the literature for the above three features. These detectors are not mutually exclusive and/or are too expensive for practical applications. We believe that the multiresolution wavelet approach proposed in Sjögreen & Yee [21] is capable of detecting all of these flow features, resulting in three distinct sensors. If chosen properly, one multiresolution wavelet basis function might be able to detect all three features. For an optimum choice, one might have to use more than one type of wavelet basis functions but at the expense of an increase in CPU requirements. Some incremental studies into the use of entropy splitting and the application of these sensors were illustrated in [31, 21, 22, 24, 23, 16]. Here, additional tools are illustrated together with highlights of some examples. An adaptive numerical dissipation model illustrating some of the proposed ideas will be described in the next section. Full implementation of the complete treatment of the numerical approach (including grid adaptation) discussed in Section 1 to complex realistic multiscale problems is in progress.

5. Numerical Examples

This section illustrates the power of entropy splitting, the difference in performance of linear and nonlinear (with sensor controls) filters and the combination of both types of filters with adaptive sensor controls. We use the same notation as in [30, 31, 22]. The artificial compression method (ACM) and wavelet filter schemes using a second-order nonlinear filter with sixth-order spatial central interior scheme for both the inviscid and viscous flux derivatives are denoted by ACM66 and WAV66. See [30, 31, 22] for the forms of these filter schemes. The same scheme without filters is denoted by CEN66. The scheme using the fifth-order WENO for the inviscid flux derivatives and sixth-order central for viscous flux derivatives is denoted by WENO5. Computations using the standard fourth-order Runge-Kutta temporal discretization are indicated by appending the letters "RK4" as in CEN66-RK4. ACM66 and WAV66 use the Roe's average state and the van Leer limiter for the nonlinear numerical dissipation portion of the filter. The wavelet decomposition is applied in density and pressure, and the maximum wavelet coefficient of the two components is used. The nonlinear numerical dissipation is switched on wherever the wavelet analysis gives a Lipschitz exponent [21] less than 0.5. Increasing this number will reduce oscillations, at the price of reduced accuracy (see [21] for other possibilities). Computations

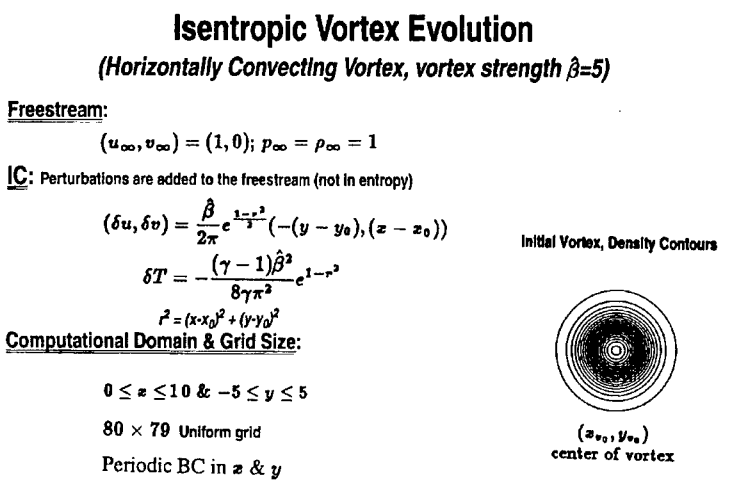

Figure 5.1. Vortex convection problem description.

using entropy splitting are indicated by appending the letters "ENT" as in WAV66-RK4-ENT. Computations using an eighth-order linear dissipation filter are indicated by appending the letters "D8" as in WAV66-RK4-D8. In order not to introduce additional notation, inviscid flow simulations are designated by the same notation, with the viscous terms not activated.

5.1. A 2-D VORTEX CONVECTION MODEL [30, 31, 21, 23]

The onset of nonlinear instability of long-time numerical integration, the benefit of the entropy splitting and the difference in performance of linear and nonlinear numerical dissipations in improving nonlinear stability for a horizontally convecting vortex (see Fig. 5.1) can be found in in [30, 31, 21, 23]. We summarize the result here.

To show the onset of nonlinear instability, the 2-D perfect gas compressible Euler equations are approximated by CEN66-RK4 with periodic boundary conditions imposed using a 80×79 grid with the time step $\Delta t = 0.01$. Since this is a pure convection problem, the vortex should convect without any distortion if the numerical scheme is highly accurate and non-dissipative. Although CEN66-RK4 is linearly stable, the test problem is nonlinear and instability eventually sets in. Almost perfect vortex preservation is observed for up to 5 periods of integrations (5 times after the vortex has convected back to the same position - time = 50). Beyond 5 periods the solution becomes oscillatory, and blows up before the completion of 6 periods. The blow up is associated with an increase in entropy [23]. If we instead use the entropy-split form of the approximation (CEN66-RK4-ENT) with a split parameter $\beta = 1$, almost perfect vortex preservation for up to 40 periods can be obtained. The computation remains stable for up to 67 periods before it breaks down. The time history of the L^2 entropy norm and density contours of the solution after 5, 10, 30 and 67 periods using CEN66-RK4-ENT is shown in Figs. 5.2 and 5.3. The norm is decreasing, although the instabilities break down the solution after 67 periods. Using the second-order nonlinear filter without splitting (ACM66-RK4 or WAV66-RK4), the solution remains stable beyond 67 periods. However, the numerical solution gradually starts to diffuse after 20 periods. If we use the nonlinear filter in conjunction with entropy splitting (ACM66-RK4-ENT or WAV66-RK4-ENT), almost perfect vortex preservation can be obtain for up to 120 periods using a split parameter $\beta = 1$ [31].

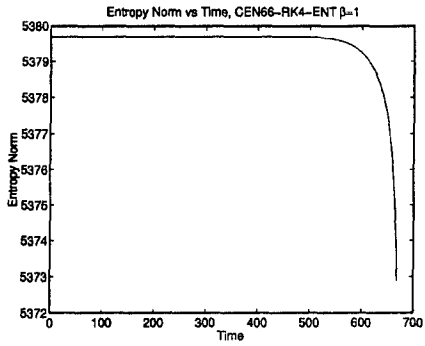

Figure 5.2. Entropy norm history of CEN66-ENT: entropy split parameter $\beta = 1$ and 80×79 grid.

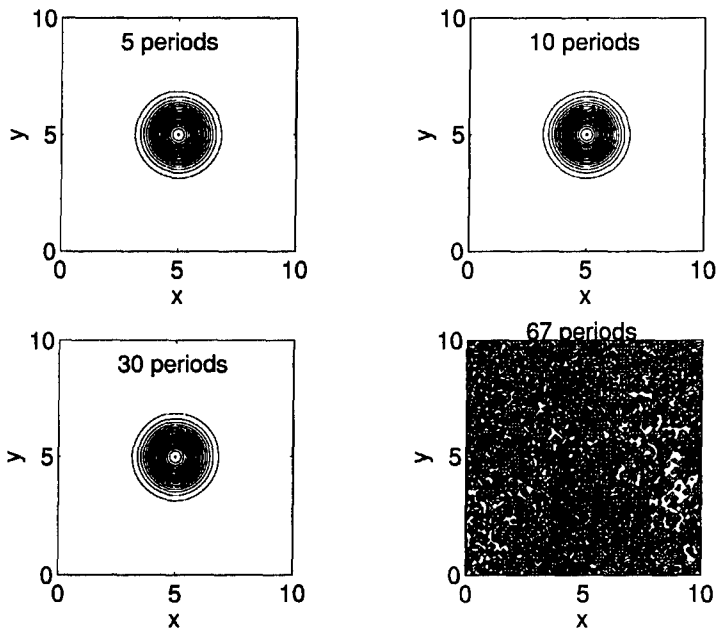

Figure 5.3. Density Contours of CEN66-ENT: entropy split parameter $\beta = 1$ and 80×79 grid.

The density contours of the solution after 5, 10, 200 and 300 periods for the unsplit ($\beta = \infty$) computation using the eighth-order linear dissipation (CEN66-RK4-D8) are shown in Fig. 5.4. The linear dissipation term $(-dh^7(D_+D_-)^4U_j)$ with grid spacing h was added to the sixth-order base scheme to discretize the convection terms. The parameter d is a given constant ($d = 0.0002$) and is scaled with the spectral radius of the Jacobian of the flux function, and D_+ and D_- are the

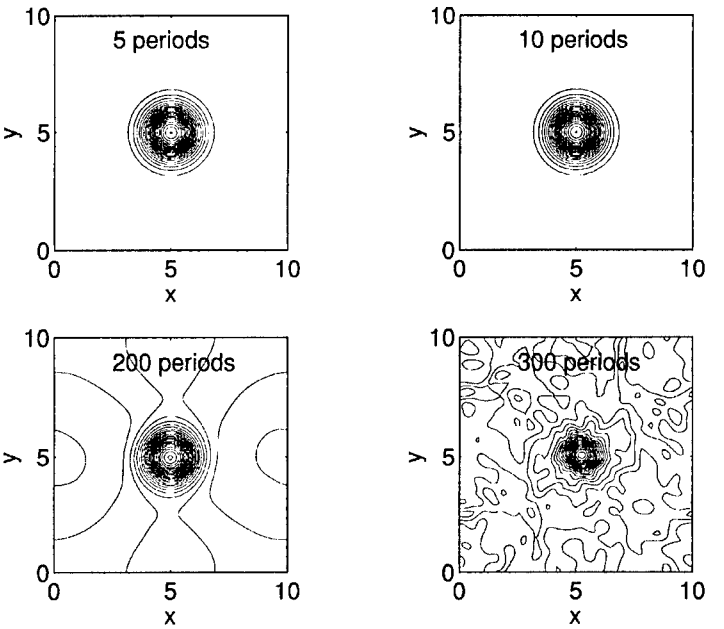

Figure 5.4. Density contours of CEN66-RK4-D8 using 80 × 79 grid.

forward and backward difference operators, respectively. This numerical dissipation is applied as part of the scheme and not as a post processing filter. The computation can be run for 300 periods without breakdown. However, serious degradation of accuracy occurs after 250 periods. For this particular problem, the CEN66-RK4-D8 out performed the ACM66-RK4-ENT and WAV66-RK4-ENT using $\beta = 1$. Perhaps using a higher than third-order nonlinear filter might improve the performance of the ACM66-RK4-ENT and WAV66-RK4-ENT at the expense of an increase in CPU.

5.2. DNS OF 3-D COMPRESSIBLE TURBULENT CHANNEL FLOW [19]

To obtain an accurate turbulent statistics, very long-time integration and highly accurate methods are required for this DNS computation. This numerical example illustrates the power of entropy splitting. The computation employed the SBP-satisfying boundary difference operator with the fourth-order central interior scheme applied to the split form of the inviscid flux derivatives CEN44-RK4-ENT with $\beta = 4$. The fluid mechanics of this 3-D wall bounded isothermal compressible turbulent channel flow has been studied in some detail by Coleman et al. [4]. They showed that the only compressibility effect at moderate Mach numbers comes from the variation of fluid properties with temperature. They used a uniform body force term to drive the flow, but recommended the constant pressure gradient approach which was adapted by Sandham & Yee [19]. For simplicity, the fixed pressure gradient problem rather than the constant mass flow problem was solved using fixed fluid properties. Thus only the wall shear stress and mass flow rate vary during the simulation. A Mach number of 0.1 is chosen, based on friction velocity and sound speed corresponding to the fixed wall temperature. Channel half

width h, friction velocity u_τ, wall temperature and bulk (integrated) density are the normalizing quantities for non-dimensionalization with a Reynolds number of 180. Grid refinement studies (three grids) were conducted and comparisons were made with results from incompressible flow spectral method calculations using the same computational box size and the finest of the three grids. Very good agreement was obtained. In addition, using the same uniform body force term, computational box and grid size as in Coleman et al., excellent agreement was also obtained with the Coleman et al. spectral compressible Navier-Stokes computation. What is interesting is that this simulation did not require filtering, upwinding, or additional numerical dissipation for shock free compressible turbulence computations. Moreover, this high order method can be efficiently extended to general geometries [28]. Using CEN44-RK4-ENT ($\beta = 4$) together with a so called Laplacian viscous term formulation, Sandham & Yee [19] demonstrated a robustness down to very coarse resolutions, comparable with the best incompressible turbulent flow solvers incorporating de-aliasing and skew-symmetric formulation of the convection terms. For the same 3-D problem, WENO5 is more than six times as expensive yet more diffusive than the present scheme using the same temporal discretization. Without the use of the entropy splitting of the inviscid flux derivatives and Laplacian right hand side formulation, using the same CFL number, the CEN44-RK4 solutions diverge for all three grids before meaningful turbulence statistics can be obtained. In view of the spurious high-frequency-oscillation-producing nonlinear instability nature of central schemes and the past experience in incompressible turbulence simulations, in the absence of entropy splitting and Laplacian formulation, the present calculations might not even be possible with much higher resolution grid.

For the performance of ACM66-RK4, WAV66-RK4 and WENO5-RK4 on a spatially or a time-developing mixing layer problem containing shock waves, see [31, 21].

5.3. MULTISCALE COMPLEX UNSTEADY VISCOUS COMPRESSIBLE FLOWS [22, 24]

Extensive grid convergence studies using WAV66-RK4 and ACM66-RK4 for two complex highly unsteady viscous compressible flows are given in [22, 24]. The first flow is a 2-D complex viscous shock/shear/boundary-layer interaction. This is the same problem and flow conditions studied in Daru & Tenaud [5]. The second flow is a supersonic viscous reacting flow concerning fuel breakup. More accurate solutions were obtained with WAV66-RK4 and ACM66-RK4 than with WENO5-RK4, which is nearly three times as expensive. To illustrate the performance of these nonlinear filter schemes, the first model is considered. The ideal gas compressible full Navier-Stokes equations with no slip BCs at the adiabatic walls are used. The fluid is at rest in a 2-D box $0 \leq x, y \leq 1$. A membrane with a shock Mach number of 2.37 located at $x = 1/2$ separates two different states of the gas. The dimensionless initial states are

$$\rho_L = 120, \quad p_L = 120/\gamma; \qquad \rho_R = 1.2, \quad p_R = 1.2/\gamma, \tag{5.1}$$

where ρ_L, p_L are the density and pressure respectively, to the left of $x = 1/2$, and ρ_R, p_R are the same quantities to the right of $x = 1/2$. $\gamma = 1.4$ and the Prandtl number is 0.73. The two Reynolds numbers considered are 200 and 1000. The viscosity is assumed to be constant and independent of temperature, so Sutherland's law is not used. The velocities and the normal derivative of the temperature at the boundaries are set equal to zero. This is done by leaving the value of the density obtained by the one sided difference scheme at the boundary unchanged, and updating the energy at the boundary to make the temperature derivative equal to zero.

At time zero the membrane is removed and wave interaction occurs. An expansion wave and a shock are formed initially. Then, a boundary layer is formed on the lower boundary behind the right going waves. After reflection, the left going shock wave interacts with the newly formed boundary layer, causing a number of vortices and lambda shocks near the boundary layer. Other kinds of layers remain after the shock reflection near the right wall. The complexity of this highly unsteady shock/shear/boundary-layer interactions increases as the Reynolds number increases.

For illustration, here we show the difficult case of Reynolds number $Re = 1000$. The computations stop at the dimensionless time 1 when the reflected shock wave has almost reached the middle of the domain, $x = 1/2$. The numerical results discussed here are at time 1 with uniform Cartesian grid spacings as described by Daru and Tenaud. Due to symmetry, only the lower half of the domain is used in the computations; symmetry BCs are enforced at the boundary $y = 1/2$. Figure 5.5 shows the comparison of a second-order MUSCL using a second-order Runge-Kutta method (MUSCL-RK2) with WAV66-RK4, ACM66-RK4 and WENO5-RK4 using a 1000×500 grid. Comparing with the converged solution of WAV66-RK4 and ACM66-RK4 using 3000×1500 (see bottom of figure) and 4000×2000 grids (see [22]), one can conclude that WAV66-RK4 exhibits the most accurate result among the 1000×500 grid computations. We note that, for this Reynolds number, the unsteady problem is extremely stiff, requiring very small time steps and very long-time integrations before reaching the dimensionless time of 1.

5.4. AN ADAPTIVE NUMERICAL DISSIPATION MODEL FOR 1-D SHOCK-TURBULENCE INTERACTIONS

In classical CFD codes, a second order accurate base method is used together with two constant strength linear numerical dissipation terms. One linear fourth-order dissipation is used everywhere except near shocks/shears/steep-gradients to remove nonlinear instabilities. It does not affect the second order accuracy of the base scheme. The second dissipation term is a second-order linear dissipation, which affects the order of accuracy, but is only switched on near discontinuities, and/or steep unresolved gradients using a gradient sensor. The sensor used cannot distinguish the different flow features distinctly and is not accurate enough for turbulent statistics and long-time acoustic computations, unless extreme grid refinement is employed.

In analogy with the aforementioned classical methods, a more advanced numerical dissipation model with improved flow feature extraction sensors for high order central schemes is proposed. Here, we consider a dissipation model with two parts. One part is a nonlinear filter ([30]) and the second part is a high order linear numerical dissipation term modified at boundaries to become a semi-bounded operator, see [20, 23]. The wavelet dissipation control sensor developed in [21] is used as the flow feature detector. The sensor is computed from the wavelet estimate of the Lipschitz exponent α of the density and pressure in the flow field. Below we present a filter model for 1-D shock/turbulence interactions.

A Filter Model: Using a suitable wavelet basis function, the final result of the wavelet computation is a quantity, S_j, which is near zero at points x_j where the solution is smooth and near one where the solution is discontinuous. S_j depends on the Lipschitz regularity exponent of the solution. We define the filter numerical flux of the numerical dissipation operator as $H^d_{j-1/2}$.

$$H^d_{j-1/2} = \max(S_j, S_{j-1}) F^*_{j-1/2} + d_j[1 - \max(S_j, S_{j-1})](h^6 D_+(D_+D_-)^3 U_j, \qquad (5.2)$$

where $F^*_{j-1/2}$ is the flux function corresponding to the dissipative portion of a shock-capturing scheme (e.g., second order accurate TVD scheme) [30]. The first part of the filter stabilizes the scheme at shock/shear locations. The second part is an eighth-order filter which improves nonlinear stability away from shock/shear locations. Analogous eighth-order filters can be used if a sixth-order compact spatial base scheme is used [7, 27]. We switch on the high order part of the filter when we switch off the nonlinear filter. The physical quantity (e.g., local Mach number) can be used to determine the d_j parameter of this high order dissipation term.

To further increase stability properties, it is possible to use the sensor to switch on and off the entropy splitting and adjust the value of the entropy splitting parameter according to flow type and region. For this problem, however, we believe a constant $\beta = 1$ away from the shock waves is sufficient. After the completion of a full time step computation using the sixth-order

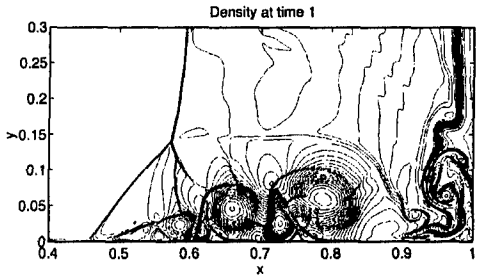

(a) MUSCL-RK2, 1000 × 500 grid

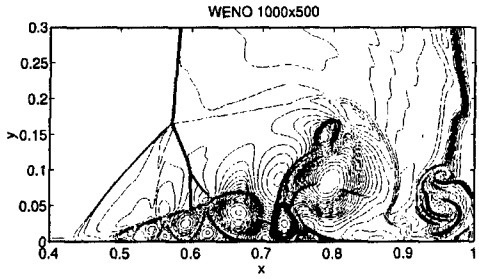

(b) WENO5-RK4, 1000 × 500 grid

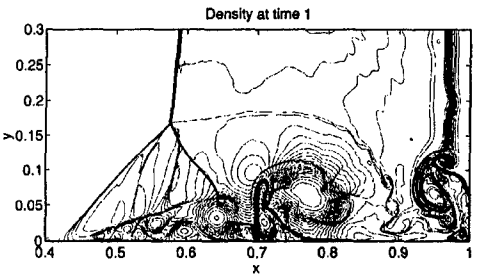

(c) WAV66-RK4, 1000 × 500 grid

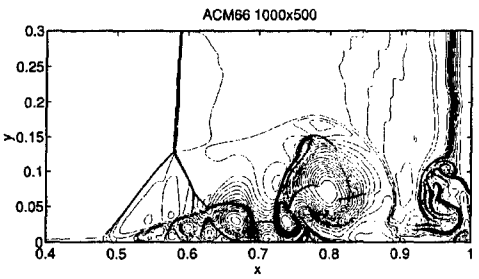

(d) ACM66-RK4, 1000 × 500 grid

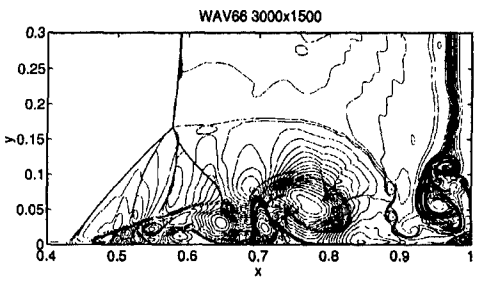

(e) WAV66-RK4, 3000 × 1500 grid

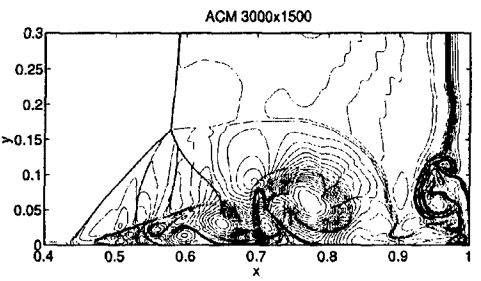

(f) ACM66-RK4, 3000 × 1500 grid

Figure 5.5. Comparison: MUSCL-RK2, WAV66-RK4, WAV66-RK4 and WENO5-RK4 for $Re = 1000$. Density contours using 1000 × 500 and 3000 × 1500 grids.

base scheme (denoting the solution by $\widehat{U}_j$), we filter this solution by

$$U_j^{n+1} = \widehat{U}_j + \frac{\Delta t}{h}[H^d_{j+1/2} - H^d_{j-1/2}]. \tag{5.3}$$

Here the filter numerical fluxes $H^d_{j\pm 1/2}$ are evaluated at $\widehat{U}$.

The Wavelet Sensor: The wavelet sensor estimates the Lipschitz exponent of a grid function f_j (e.g., the density and pressure). The Lipschitz exponent at a point x is defined as the largest

α satisfying

$$\sup_{h\neq 0}\frac{|f(x+h)-f(x)|}{h^{\alpha}}\leq C, \tag{5.4}$$

and this gives information about the regularity of the function f where small α means poor regularity. For a C^1 wavelet function ψ with compact support, α can be estimated from the wavelet coefficients, defined as

$$w_{m,j} =< f, \psi_{m,j} >= \int f(x)\psi_{m,j}(x)dx, \tag{5.5}$$

where

$$\psi_{m,j} = 2^m \psi\Big(\frac{x-j}{2^m}\Big) \tag{5.6}$$

is the wavelet function $\psi_{m,j}$ on scale m located at the point j in space. This definition gives a so called redundant wavelet, which gives (under a few technical assumptions on ψ) a non-orthogonal basis for L^2. It is possible to prove that the coefficients $\max_j |w_{m,j}|$ in a neighborhood of j_0 decay as $2^{m\alpha}$ as the scale is refined, where α is the Lipschitz exponent at j_0. In practical computation, we have a smallest scale, determined by the grid size. We evaluate $w_{m,j}$ on this scale, m_0, and a few coarser scales, m_0+1, m_0+2, and estimate the Lipschitz exponent at the point j_0 by a least square fit to the line [21]

$$\max_{j \text{ near } j_0} \log_2 |w_{m,j}| = m\alpha_{j_0} + c. \tag{5.7}$$

For the numerical experiments, the wavelet coefficient $w_{m,j}$ is computed numerically by a recursive procedure, which is a second-order B-spline wavelet or a modification of Harten's multiresolution scheme [21]. The sensor we use in the computations is

$$S_j = \tau(\alpha_j), \tag{5.8}$$

where

$$\tau(\alpha_j) = \begin{cases} 1 & \alpha_j \leq 0.5 \\ 0 & \alpha_j > 0.5. \end{cases} \tag{5.9}$$

The dissipative model (5.2) is used to solve a simple, yet difficult, 1-D compressible inviscid shock-turbulence interaction problem with initial data consisting of a shock propagating into an oscillatory density. The initial data are given by

$$(\rho_L,\ u_L,\ p_L) = (3.857143,\ 2.629369,\ 10.33333) \tag{5.10}$$

to the left of a shock located at $x=-4$, and

$$(\rho_R,\ u_R,\ p_R) = (1+0.2*\sin(5*x),\ 0,\ 1) \tag{5.11}$$

to the right of the shock where u is the velocity. Fig. 6.6 show the comparison between a second-order MUSCL-RK2 with a sixth-order central scheme and the aforementioned numerical dissipation model using RK4 as the time discretization (WAV66-RK4-D8). The parameter $d = 0.002$ is scaled with the spectral radius of the Jacobian of the flux function. Note that the eighth-order dissipation is a filter, and is different from the CEN66-D8 used in Section 5.1 where the dissipation is part of the scheme. Solution using a second-order uniformly non-oscillatory (UNO) scheme on a 4000 uniform grid is used as the reference solution (solid lines on the first three subfigures). The bottom of the right figures show the density and Lipschitz exponent distribution for the WAV66-RK4-D8 using 400 grid points. Comparing our result with the most accurate computation found in the literature for this problem, the current approach is highly efficient

and accurate using only 800 grid points without grid adaptation or very high order shock-capturing scheme. For the present computation, the WAV66-RK4-D8 consumed only slightly more CPU than the second-order scheme MUSCL-RK2. With the eighth-order dissipation filter turned off (i.e., only the nonlinear filter remains - WAV66-RK4), the computation is not very stable unless a finer grid and smaller time step is used. Turning on the entropy splitting away from the shocks helps to reduce the amount of the eighth-order dissipation coefficient [33].

6. Concluding Remarks

A general framework for the design of an adaptive low dissipative high order scheme is presented. The approach is applicable to a wide spectrum of flow problems. However the demand on the overall numerical approach for nonlinear stability and accuracy is much more stringent for long-time integration of complex multiscale shock/shear/turbulence/acoustics interactions and numerical combustion problems. Robust classical numerical methods for less complex flow physics are not suitable or practical for such applications. The present approach is designed expressly to address such flow problems and computational challenges. The incremental studies to illustrate the performance of the approach are summarized. Extensive testing and full implementation of the approach is forthcoming. The results shown so far are very encouraging.

References

1. A. Arakawa, *Computational Design for Long-Term Numerical Integration of the Equations of Fluid Motion: Two-Dimensional Incompressible Flow. Part I*, J. Comput. Phys., **1** (1966), pp. 119–143.
2. G. A. Blaisdell, *Numerical Simulation of Compressible Homogeneous Turbulence*, PhD Thesis, Stanford University, 1991.
3. M.H. Carpenter, J. Nordstrom and D. Gottlieb, *A Stable and Conservative Interface Treatment of Arbitrary Spatial Accuracy*, ICASE Report 98-12, 1998.
4. G.N. Coleman, J. Kim, J. and R. Moser *A Numerical Study of Turbulent Supersonic Isothermal-Wall Channel Flow, J. Fluid Mech.* **305**, (1995), pp. 159-183.
5. V. Daru and C. Tenaud, *Evaluation of TVD High Resolution Schemes for Unsteady Viscous Shocked Flows*, Computers Fluids, **30** 89–113 (2000).
6. P.F. Fischer and J.S. Mullen, *Filter-Based Stabilization of Spectral Element Methods*, Argonne National Lab. Report, August 4, 1999.
7. D.V. Gaitone and M.R. Visbal, *Further Development of a Navier-Stokes Solution Procedure Based on Higher-Order Formulas*, AIAA Paper 99-0557, Reno, NV, 1999.
8. M. Gerritsen and P. Olsson, *Designing an Efficient Solution Strategy for Fluid Flows*, J. Comput. Phys. **129** 245–262 (1996).
9. D. Gottlieb and J.S. Hesthaven, *Spectral Methods for Hyperbolic Problems*, J. Comput. Applied Math., **128**, 83-131 (2001).
10. A. Harten, *On the Symmetric Form of Systems for Conservation Laws with Entropy*, J. Comput. Phys. **49**, 151-164 (1983).
11. A. Harten, *Multiresolution Algorithms for the Numerical Solution of Hyperbolic Conservation Laws*, Comm. Pure Appl. Math., **48**, 1305 (1995).
12. C.W. Hirt, *Heuristic Stability Theory for Finite-Difference Equations*, J. Comput. Phys., **2** (1968), pp. 339-355.
13. M. Johansson, *Loss of High Order Spatial Accuracy due to Boundary Error Caused by Runge-Kutta Time Integration*, Technical report 2000-013, Dept. Info. Tech., Uppsala University, May 2000.
14. H.-O. Kreiss and J. Oliger, *Comparison of accurate methods for the integration of hyperbolic equations*, Tellus, **24** (1972), pp. 199-215.
15. R.W. MacCormack, *Numerical Solution of the Interaction of a Shock Wave with a Laminar Boundary Layer*, Proceedings of the 2nd Intern. Conf. on Num. Meths. in Fluid Dynamics, (1971), pp. 151-163.
16. B. Müller and H.C. Yee, *Entropy Splitting for High Order Numerical Simulation of Vortex Sound at Low Mach Numbers*, Proceedings of the 5th Internat. Conf. on Spectral and High Order Methods, Uppsala, Sweden, June 11-15, 2001.
17. P. Olsson and J. Oliger, *Energy and Maximum Norm Estimates for Nonlinear Conservation Laws*, RIACS Technical Report 94.01 (1994).
18. P. Olsson, *Summation by Parts, Projections, and Stability. III*, RIACS Technical Report 95.06 (1995).
19. N. D. Sandham and H.C. Yee, *Entropy Splitting for High Order Numerical Simulation of Compressible Turbulence*, RIACS Technical Report 00.10, June 2000, NASA Ames Research Center; Proceedings of the First International Conference on CFD, July 10-14, 2000, Kyoto, Japan.
20. B. Sjögreen, *High Order Centered Difference Methods for the Compressible Navier-Stokes Equations*, J.

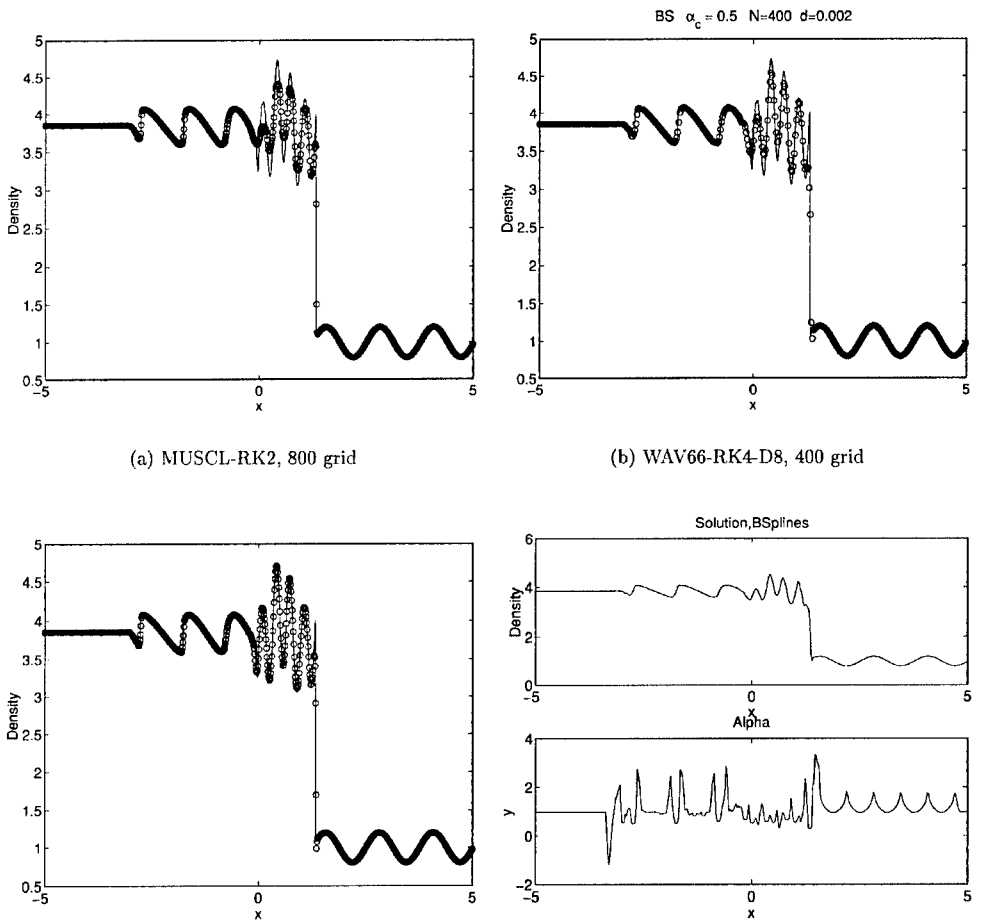

(a) MUSCL-RK2, 800 grid

(b) WAV66-RK4-D8, 400 grid

(c) WAV66-RK4-D8, 800 grid

(d) Density & Lipschitz Exponent Distributions, WAV66-RK4-D8, 400 grid

Figure 6.6. Comparison and Lipschitz exponent distribution of WAV66-RK4-D8, second-order B-spline wavelet.

Comput. Phys., **117** (1995), pp. 67–78.

21. B. Sjögreen and H. C. Yee *Wavelet Based Adaptive Numerical Dissipation Control for Shock-Turbulence Computation*, RIACS Report 01.01, NASA Ames research center (Oct 2000).
22. B. Sjögreen and H. C. Yee, *Grid Convergence of High Order Methods for Multiscale Complex Unsteady Viscous Compressible Flows*, RIACS Report 01.06, April, 2001, NASA Ames Research Center; AIAA 2001-2599, Proceedings of the 15th AIAA CFD Conference, June 11-14, 2001, Anaheim, CA.
23. B. Sjögreen and H.C. Yee *On Entropy Splitting, Linear and Nonlinear Numerical Dissipations and Long-Time Integrations*, Proceedings of the 5th Internat. Conf. on Spectral and High Order Methods, Uppsala, Sweden, June 11-15, 2001.
24. B. Sjögreen and H. C. Yee, *Low Dissipative High Order Numerical Simulations of Supersonic Reactive Flows*, RIACS Report 01-017, NASA Ames Research Center (May 2001); Proceedings of the ECCOMAS Computational Fluid Dynamics Conference 2001, Swansea, Wales, UK, September 4-7, 2001.
25. B. Strand, *Summation by Parts for Finite Difference Approximations for d/dx*, J. Comput. Phys. **110** (1994), pp. 47–67.

26. E. Tadmor, *Skew-Self Form for Systems of Conservation Laws*, J. Math. Anal. Appl., **103** (1984), pp. 428–442.
27. R. Vichnevetsky, *Numerical Filtering for Partial Differencing Equations*, Numerical Applications Memorandum, Rutgers University, NAM 156 (1974).
28. M. Vinokur and H.C. Yee, *Extension of Efficient Low Dissipative High Order Schemes for 3-D Curvilinear Moving Grids*, NASA TM 209598, June 2000.
29. H.C. Yee, P.K. Sweby, *Dynamics of Numerics & Spurious Behaviors in CFD Computations*, 7th ISCFD Conference, Sept. 15-19, 1997, Beijing, China, RIACS Technical Report 97.06, June (1997).
30. H. C. Yee, N. D. Sandham, and M. J. Djomehri, *Low Dissipative High Order Shock-Capturing Methods Using Characteristic-Based Filters*, J. Comput. Phys., **150**, 199 (1999).
31. H.C. Yee, M. Vinokur, and M.J. Djomehri, *Entropy Splitting and Numerical Dissipation*, NASA Technical Memorandum 208793, August, 1999, NASA Ames Research Center; J. Comput. Phys., **162**, 33 (2000).
32. H.C. Yee, B. Sjögreen, N.D. Sandham and A. Hadjadj, *Progress in the Development of a Class of Efficient Low Dissipative High Order Shock-Capturing Methods*, RIACS Technical Report 00.11, June, 2000; Proceedings of the CFD for the 21st Century, July 15-17, 2000 Kyoto, Japan.
33. H.C. Yee and B. Sjögreen, *Designing Adaptive Low Dissipative High Order Schemes for Long-Time Integrations*, RIACS Technical Report, in preparation (2001). An invited chapter for *Turbulent Flow Computation*," (eds. D. Drikakis & B. Geurts), Kluwer Academic Publisher.
34. S.T. Zalesak, *High Order "ZIP" Differencing of Convective Terms*, J. Comput. Phys., **40** (1981), pp. 497-508.
35. T. A. Zang, *On the Rotation and Skew-Symmetric Forms for Incompressible Flow Simulations*, Appl. Numer. Math., **7** (1991), pp. 27–40.